Simulation and Experimental Analysis of Temperature Profiles and Crosslinking in PV Module Lamination

Aksel Kaan Öz, Japan Vasani, Christian Reichel, Christine Wellens, Max Mittag, Martin Heinrich, Dirk Holger Neuhaus

***Abstract*— The lamination process plays a crucial role in the long-term reliability of photovoltaic (PV) modules. Monitoring the degree of encapsulant crosslinking in the modules can help ensure the quality of the lamination process, which is affected by factors like lamination temperature and process time. A consistent vertical temperature distribution during lamination is important for achieving uniform crosslinking across the module depth. In this study, thermocouple measurements were conducted to obtain temperature profiles and assess the degree of encapsulant crosslinking in glass-backsheet (GB) and glass-glass (GG) modules with and without cells. Four different encapsulants were analyzed, including two types of ethylene-co-vinyl acetates (EVA) and two types of polyolefin elastomers (POE). The measurements data were compared with simulations that allow to determine the temperature profile of the different layers of the module as well as the degree of crosslinking of the encapsulants over the process time. The simulation results showed good agreement with the measured values, effectively capturing the temperature trends during lamination. It was found that inadequate processing led to a crosslinking discrepancy between the front and back sides of the modules of 6.5% for EVA, and 14% for POE. To address this issue, a i) plate-plate chamber was used for GG modules or the ii) process time was extended in the plate-membrane chamber. The study also highlighted the significant influence of the cells on the degree of crosslinking, whereas the implementation of the cells decreases the crosslinking by up to 12.8%. Additionally, the simulated encapsulant crosslinking was validated against Soxhlet extraction results.**

***Index Terms*— Degree of Crosslinking, Lamination, Module Manufacturing, Simulation, PV Modules**

I. INTRODUCTION

In recent years, the photovoltaic (PV) industry has made significant advancements in cell technologies, sizes, and materials, driven by the goals of cost reduction and improved module efficiency while ensuring long operational lifetimes with minimal power degradation [1], [2], [3]. With the emergence of new cell technologies like HJT and TOPCon, different encapsulants such as POE have entered the market [4], [5], [6], [7], [8], [9]. The lamination process plays a critical role in achieving long-term reliability, ensuring robust adhesion between module layers and a sufficient degree of encapsulant crosslinking to protect the module against external stressors and environmental factors that could compromise cell integrity [10], [11], [12], [13], [14]. To optimize the lamination process for new encapsulation materials, it is essential to consider key parameters such as temperature, time, and pressure, adjusted to the specific new material combination. Achieving a consistent temperature distribution within the module, both laterally and across different layers, is also crucial [11], [15].

This paper focuses on assessing vertical temperature homogeneity during the lamination process using two methods, 1) comparing the degree of crosslinking in the encapsulant on the front and rear sides of the cell and 2) conducting thermocouple measurements to capture the temperature profile within the module. The simulation streamlines the evaluation of new bills of materials (BOM), saving valuable time and costs.

The study specifically examines the widely used encapsulants EVA and the newly more popular POE [6], [16], [17]. As there is currently no standard for the Soxhlet extraction to obtain the degree of crosslinking for POE encapsulants, we adapted our approach to align with the existing EVA standard. To validate our findings, we compare the measured degree of crosslinking and temperature profiles with two different lamination processes and with simulation results.

In summary, this research highlights the crucial role of the lamination process in achieving longevity and quality in PV modules. By investigating temperature homogeneity and by using simulations, we aim to contribute to streamlined evaluation processes of new development in module technology within the PV industry. Additionally, we share insights on the new POE material and provide an approach to obtain a more accurate degree of crosslinking with Soxhlet extraction.

II. MATERIALS AND METHODS

During experiment 1, we produced a total of eight modules in glass-glass (GG) and glass-backsheet (GB) configurations, with a size of 680 mm x 370 mm. These modules were laminated using the two different encapsulants EVA 1 and POE 1. The typical lamination process in the plate-membrane chamber

"This work was supported by the German Federal Ministry for Economic Affairs and Energy (BMWi) under the contract number 0324287C, acronym GEPARD." *(Corresponding author: Aksel Kaan Öz).*

Aksel Kaan Öz, Japan Vasani, Christian Reichel, Christine Wellens, Max Mittag, Martin Heinrich, Dirk Holger Neuhaus are with the Fraunhofer Institute for Solar Energy Systems, Department Module Technology, Heidenhofstraße 2, 79110, Freiburg im Breisgau, Germany. (e-mail: aksel.kaan.oez@ise.fraunhofer.de)

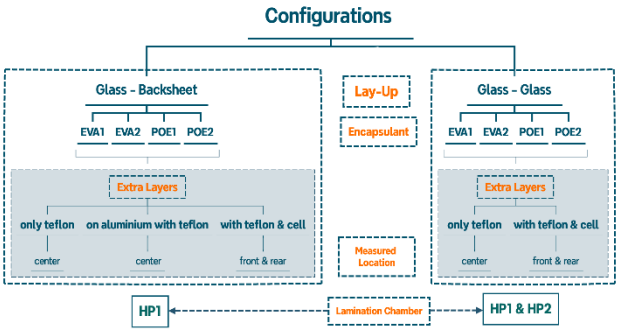

Fig. 1. Module matrix, describing the configurations and lamination chambers used in the experiment.

(HP1) was applied for both configurations (GB, GG), at Ypsator of Bürkle.

In experiment 2, we examined 20 different conditions and laminated a total of 40 modules. Sometimes on mini module level, modules are laminated on aluminum plates for easy handling, to analyze the influence of that phenomenon we also laminated some modules on aluminum to compare them with the others. The comprehensive module matrix is shown in Fig. 1. To ensure accurate results, two modules were manufactured for each case and subjected to crosslinking tests twice. To simplify the sample preparation for determining the degree of crosslinking, an additional layer of Teflon was introduced between the encapsulant and the glass or rear side layer. Furthermore, the lamination process differed for GB and GG modules. GB modules went through lamination in HP1, while GG modules were pre-processed in HP1 and then transferred to the plate-plate chamber (HP2) for crosslinking. The main distinction between HP1 and HP2 is that in HP2, the module is actively heated from both sides and is in direct contact with the heating plates, whereas in HP1, the module only contacts the bottom heat plate and receives less heat from the top side. There was also a distinct difference between the GB and GG process depending on the encapsulant used. The lamination temperature for the EVA encapsulant was 155 °C while the POE encapsulant was laminated at 150 °C. Further details about the process parameters are shown in Fig. 9

For the various lay-ups, samples for Soxhlet extraction were taken from the stages indicated in Fig. 1. The modules with cells were measured on both sides of the cell, while samples of modules without cells, referred to as "laminates," were taken from their center. The study also examined the degree of crosslinking in laminates and modules to investigate the influence of cells. The specifications of the glasses, encapsulants, and other materials used are provided in Table I in the supplementary information.

A. Soxhlet Extraction

To assess the influence of vertical temperature distribution during the lamination process, the degree of crosslinking was measured. For this purpose, we adopted the Soxhlet extraction method, —a precise yet time-intensive technique widely used for measuring the degree of crosslinking in PV modules [18], [19].

In the Soxhlet extraction, first the sample is weighted then it is placed in a stainless-steel mesh tube, which in turn is placed in a glass tube. The extraction starts by heating the solvent. The extractions are carried out by using xylene as solvent. During the extraction the solvent starts boiling and evaporates, reaching the cooling system on top of the sample where it condenses and starts to fill the glass tube in which the sample is. Once the solvent level reaches the siphon, the solvent containing the dissolved polymer flows back into the reaction flask. The whole process from heating the solvent until it is poured back to the reaction flask is called one cycle. One extraction consists of multiple cycles followed by the drying process. At the end the dissolved sample is weighted again and the Soxhlet degree of crosslinking is calculated. The Soxhlet degree of crosslinking is calculated by [18]

$$X\,(Soxhlet)[\%] = \left(\frac{M_2 - M_0}{M_1 - M_0}\right) x\ 100,\ M_2 \leq M_1 \qquad (1)$$

where "M_0" indicates the pre-determined weight of the cylindrical stainless steel mesh tube, "M_1" the total weight of the sample and its tube before the process and "M_2" the weight of the sample and its tube after being extracted and dried in a vacuum oven.

The measurements were performed using the Behrotest apparatus based on the standards outlined in IEC 62788-1-6. Each module underwent at least two sample measurements, and the results represent the mean value and standard deviation of the measurements [20].

B. DSC Measurements

DSC measurements are performed on a Q2500 DSC machine from TA instruments to determine the degree of crosslinking of the encapsulants EVA and POE for a heating rate of 5 K/min, 10 K/min, and 12 K/min. The heat flow rate is constant throughout the DSC measurements and the material is heated from -80 °C to 200 °C. The temperature, heat flux and mass of the encapsulants are measured over time to determine the encapsulation material's reaction enthalpy. The peak temperature is the maximum temperature measured during the exothermic reaction that typically occurs between 100 °C and 200 °C. The peak area is derived from the exothermic reaction using the interpolated baseline of the heat flow, calculating it for the sample and a reference. The reaction enthalpy can be calculated using the peak area as follows

$$H = \left(\frac{A_{peak}}{r_{heat}}\right) \qquad (2)$$

The DSC degree of cure (X) is determined from the reaction enthalpy of the sample material (H_{samp}) in comparison to the reaction enthalpy of a reference material (H_{ref}) according to [21]

$$X\,(DSC)[\%] = \left(\frac{H_{ref} - H_{samp}}{H_{ref}}\right) \times\ 100. \qquad (3)$$

As the degree of cure determined by the DSC is not always the maximum degree of crosslinking, a calibrated value is calculated using the maximum degree of crosslinking extracted by the Soxhlet method X_{max}. The following equation

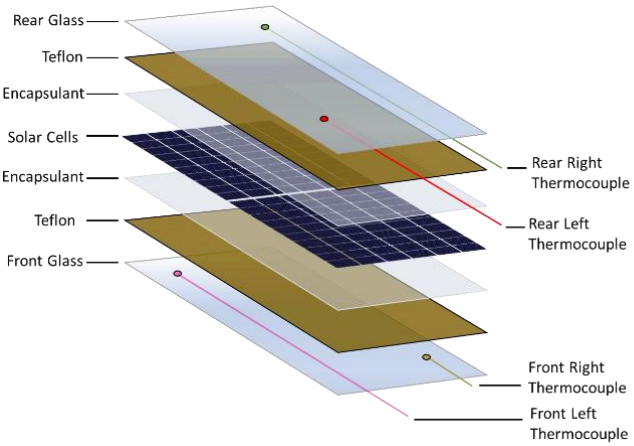

Fig. 2. Module lay-up and sensor locations for the thermocouple measurements.

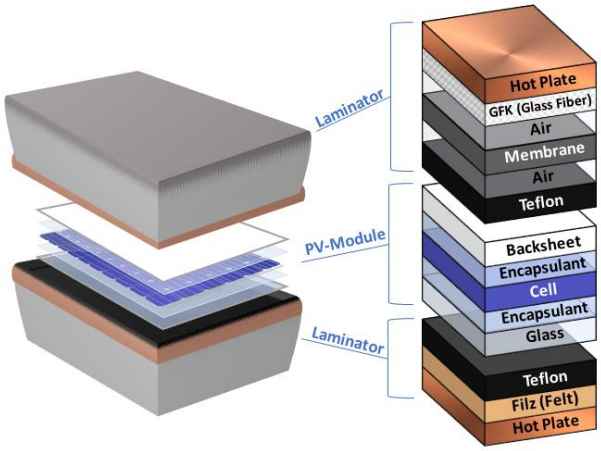

Fig. 3. Fundamental layout for simulations of the laminator including PV module.

is used to calculate the calibrated degree of crosslinking X_{calib}

$$X_{calib} = \frac{X \times X_{max}}{100}\ [\%] \qquad (4)$$

C. Thermocouple Measurements

Type K thermocouples were used to monitor the temperature dynamics during lamination in a standard-sized module (1960 mm x 1010 mm). Simultaneously, the Datapaq Q18 datalogger was used to log the temperature profile throughout the process. Four sensors were strategically positioned within the module to indicate the horizontal heat distribution uniformity and compare the heat variations between the front and rear sides Fig. 2

It is important to note that the PV module lay-up used for the thermocouple measurements slightly differed from the standard industry configuration. An additional Teflon sheet was inserted between the sensors and the encapsulant to allow for sensor reuse in different lay-ups (GB, GG) and processes (HP1 and HP1 & HP2 process). Fig. 2 shows the configuration where the sensors are placed between the inner side of the glass and the additional Teflon sheet for the GG lay-up.

D. Simulation

The degree of crosslinking of different encapsulants in GB and GG modules, as shown in Fig. 2, is modelled based on the temperature profile during the lamination process. To this end, a thermal model is developed to determine the one-dimensional temperature distribution within the different module layers caused by the heating plate in the lamination process [22]. In addition, the model is further extended to also take layers of the laminator into account, see Fig. 3. Numerical differentiation is used to calculate the energy balance between the different layers and obtain the temperature distribution of each layer. The thermal properties and the thickness of the different layers are shown in Table I in the supplementary information based on the data provided in [25-39].

For the simulation of the crosslinking degree, the thermal behaviour of the encapsulant needs to be modelled first. This simulation is based on the following steps (see Fig. 4, left side). Firstly, the simulation is run with DSC input parameters such as heat flow and temperature to determine the peak temperature and calculate the peak area of the exothermic chemical reaction. Secondly, the calculation of the reaction enthalpy from the peak area is performed. Thirdly, Soxhlet measurements are used to calculate the maximum degree of crosslinking of the encapsulants EVA and POE and calibrate the DSC values. Fourthly and lastly, a kinetic analysis is applied to calculate the activation energy, which is then followed by the calculation of the degree of crosslinking of the encapsulant in dependence of the temperature profile in the lamination process, following the method used for electrically conductive adhesives [23], [24].

The Friedman differential isoconversional technique is considered to be the most accurate model to determine the energy (E_α) because it utilizes both conversion α and conversion rate data (dα/dt). Friedman's equation is obtained by taking the logarithm of both sides of the equation shown in [40], [43]

$$\ln\left(\beta \frac{d\alpha}{dt}\right) = \ln[A\, f(\alpha)]\ \frac{-E_\alpha}{RT} \qquad (5)$$

Hence, the slope ($-E_\alpha/R$) of a plot of ln(dα/dt) against the reciprocal temperature (1/T) at constant conversion for a given set of heating rates yields the apparent activation energy E_α. The activation energy and temperature profile of the encapsulation material are used to acquire the final results of the degree of crosslinking of the encapsulant for a certain lamination process. The process flow of the calculation of degree of crosslinking is shown in Fig. 4.

III. RESULTS AND DISCUSSION

In this section, first the Soxhlet extraction parameters are varied to optimize the method for POE. The degree of crosslinking is then analyzed for various conditions, and the simulation results are presented.

A. Optimization of the Soxhlet Extraction for POE

To optimize the Soxhlet extraction method for POE, different extraction durations were analyzed to determine the saturation point of the degree of crosslinking curve.

The results depicted in Fig. 5, indicate that a longer extraction duration is necessary to reach the saturation point for

This article has been accepted for publication in IEEE Journal of Photovoltaics. This is the author's version which has not been fully edited and content may change prior to final publication. Citation information: DOI 10.1109/JPHOTOV.2024.3414117

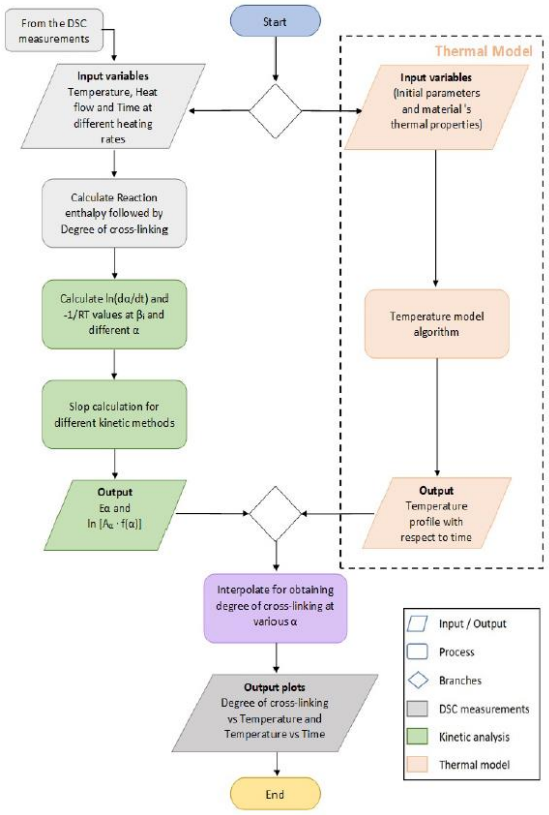

Fig. 4: Process flow for the calculation of degree of crosslinking of the encapsulant.

POE 1 compared to the standard EVA extraction where the extraction time is usually 8-12 hours depending on the degree of crosslinking of the sample, whether this is below or higher than 70%. [17], [44].

It should be noted that this curve might shift, and different extraction durations might be required depending on the specific POE used in the module's BOM. In general, it is important to consider the various material properties that influence the degree of crosslinking. Oreski et al. have highlighted the wide range of material characteristics of POEs currently available in the market [45].

As a result, the POE extraction duration for this study was set as 16 hours. All Soxhlet extractions for POE in the upcoming sections were conducted with these parameters.

B. Comparison of Front and Rear Degree of Crosslinking

In experiment 1, the process in HP1 was employed for all laminates and modules (EVA 1, POE 1). In experiment 2, different EVAs and POEs were tested, and the laminator process was alternated between the HP1 one and the HP1+HP2 one based on the module lay-up. The results obtained are presented in Fig. 6.

Fig. 6 (a) demonstrates a significant reduction in crosslinking for all GG modules in experiment 1, compared to the GB modules. The observed 6.5% (EVA) and 14% (POE) differences in crosslinking between the rear and front side of the GG modules suggest a temperature difference between the two sides. This difference is attributed to the lamination process used, which was performed in the HP1 (membrane-plate chamber), with direct heating only from the front side. To

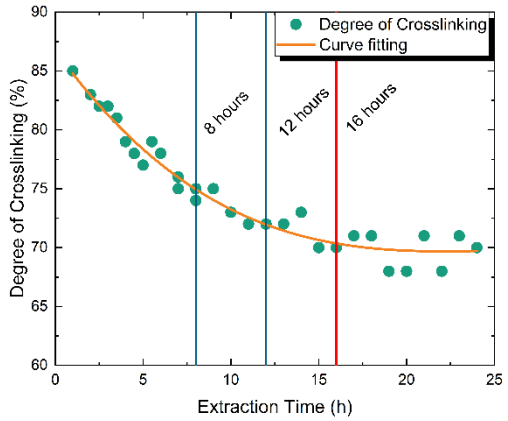

Fig. 5. Degree of crosslinking vs. extraction duration for POE 1.

enhance the heat transport and crosslinking uniformity in GG modules, an extended process duration in HP1 or transitioning to HP2 (plate-plate chamber) is recommended (Fig. 9 (b)).

Fig. 6 (b) shows a reduced difference in crosslinking between the front and rear side compared to Fig. 6 (a). This improvement can be attributed to GG modules being laminated using a combination of HP1 and HP2, which facilitates better heat transport and crosslinking uniformity. Notably, EVA 2 consistently exhibits lower crosslinking compared to EVA 1, potentially due to differences in the amount of curing agents in the encapsulant or the suitability of the process for EVA 1 [16]. A similar trend is also observed for the POEs, especially for the glass-glass layup, where POE 2 exhibits around 12% higher degree of crosslinking compared to POE 1.

C. Crosslinking in Laminates versus Modules

Considering the lower degrees of crosslinking observed in modules (with cells) compared to laminates (without cells), we further investigated the influence of cells on the degree of crosslinking. While laminates were sampled from the center, module sampling was constrained by the presence of cells. The degree of crosslinking for GB and GG laminates and modules is shown in Fig. 7. The values for modules, represent the average degree of crosslinking from the front and rear side. Furthermore, the influence of aluminum plates was also examined (Fig. 8) as for the fabrication of mini-modules aluminum plates are often used as handling support for smaller modules.

Fig. 7 illustrates the crosslinking degrees for GB and GG modules, revealing differences ranging from 3.5% to 12.75% when comparing laminates to modules. The graph highlights a reduction in crosslinking after inserting cells for all cases. Both POEs were more affected by this phenomenon than the EVAs. The degree of crosslinking decreased by 11.13% and 10.34% for GB layup and 12.63% and 7% for GG layup with POE1 and POE2, respectively.

Notably, the difference remained relatively stable (around 4%) with EVA1, while EVA2 was more influenced by the lay-up. The reason that the POEs are more effected by this might be that they had already a lower degree of crosslinking before adding the cells than the EVA samples.

Laminating the mini modules on top of an aluminum plate decreases the degree of crosslinking (see Fig. 8 in

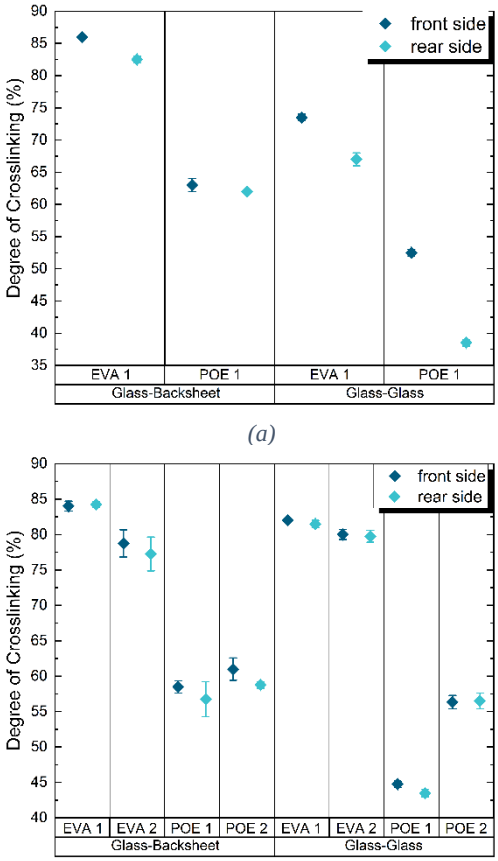

Fig. 6. Comparison of the degree of crosslinking on the front and rear side of the modules, (a) experiment 1 in HP1, (b) experiment 2 in HP1+HP2.

supplementary section). This is attributed to the heat capacity of the aluminum plate that acts as an additional layer between the heat plate and the module. Therefore, this factor should be considered when setting up processes for or comparing mini-modules to standard-sized modules without an aluminum plate. This is especially important when a new BOM is tested on mini modules first before moving to full size modules.

D. Temperature Profile during Lamination

The temperature profile during lamination was investigated to examine the differences in the crosslinking between the front and rear side of the cells in the module. The results of the thermocouple measurements and simulations for the lamination processes conducted in the HP1 and HP1+HP2 chambers, along with their lamination parameters, are compared in Fig 9. At both processes, the first step of lamination, the evacuation, occurs in the HP1 chamber. Additionally, the curing step of the GB modules also takes place in the HP1 chamber, while for the GG modules, the curing primarily occurs in the HP2 chamber after transferring the module from HP1 to HP2 in process 2. Lastly, both types of modules enter the cooling press (CP). The chamber location of the modules during the measurements is indicated on the figures while the area between the black dash dot lines shows the transfer duration from one chamber to another.

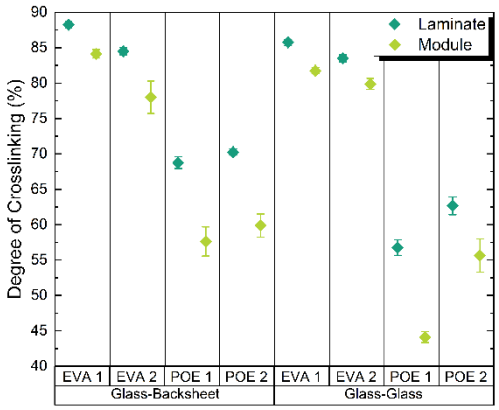

Fig. 7. Influence of solar cells on the degree of crosslinking, where "Laminates" indicate lay-ups without cells whereas "Modules" include cells.

Both the simulated temperature and thermocouple measurements demonstrate consistency in temperature evolution. For the GB process, there is a certain temperature rise observed until 240 seconds, followed by a faster increase in temperature and a smoother curve. The first 240 seconds are the evacuation phase where the pins are up. The faster increase in temperature after 240 seconds is related to the direct contact of the laminate with the hotplate as the pins go down in the curing phase and the module gets in direct contact with the heating plate, which provides a faster heat transfer.

Both the simulated temperature and thermocouple measurements demonstrate consistency in temperature evolution. For the GB process, there is a certain temperature rise observed until 240 seconds, followed by a faster increase in temperature and a smoother curve. The first 240 seconds are the evacuation phase where the pins are up. The faster increase in temperature after 240 seconds is related to the direct contact of the laminate with the hotplate as the pins go down in the curing phase and the module gets in direct contact with the heating plate, which provides a faster heat transfer.

After 750 seconds, the module is transferred from HP1 to the cooling press CP for cooling. There is a small delay before rapid cooling due to the transfer between the different chambers. This phenomenon takes around 50 ±10 seconds in this process and can be observed between the 750 and 800 seconds (area between the black dash dot lines).

The results indicate that the length of the process is nearly optimal. The maximum temperatures reached by the sensors on the front and rear sides are 153.9 °C and 153.4 °C, respectively for glass backsheet modules. The simulation values are 154.8 °C and 154.9 °C, while the set temperature of the process was 155 °C.

An interesting observation for GB modules is that the rear side of the module initially has a higher temperature compared to the front side. This phenomenon is also observed in the simulation, but to a much lesser extent. The reason for that is that till 240 seconds there is no direct contact on both sides of the module as it lies on the pins. Hence, the heat transfer through the backsheet is faster as the membrane is in direct contact to the rear side compared to the heat transfer though the glass on the front side as it is in contact with air and pins only.

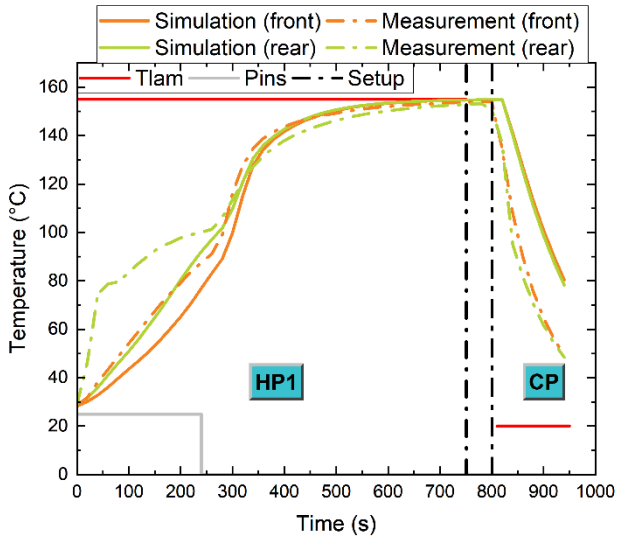

(a)

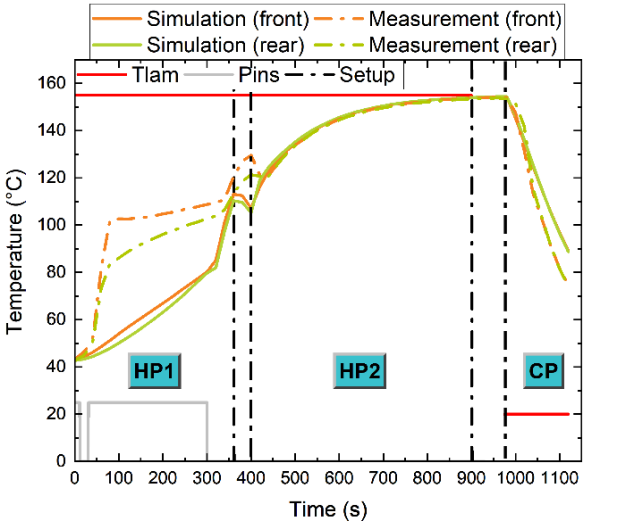

(b)

Fig. 9. Temperature profile and lamination process parameters during the lamination process for (a) a glass-backsheet module, (b) a glass-glass module

Fig. 9 (b) shows that the temperature on the front side of the GG module is higher compared to the rear side, which is different from the GB module lay-up. This difference can be attributed to the short direct contact with the heating plate of the laminate at the beginning of the process when the pins are down for few seconds and that at this time, we have the same thermal characteristics on both sides of the module by using the GG layup.

As in Fig. 9 (a), the influence of the pins and the delay in cooling during the transfer to the CP can be observed in Fig 9 (b). Here the evacuation duration on the pins is 300 seconds, followed by an increase in temperature reaching a peak around 360 seconds. Afterwards the module is transferred from HP1 to HP2. Once the GG enters the HP2 chamber an increase in temperature is observed, since it is heated actively from both sides. That provides a better heat transfer and helps that a homogeneous temperature is reached on both sides of the module. In this phase the temperature gap from HP1 closes and

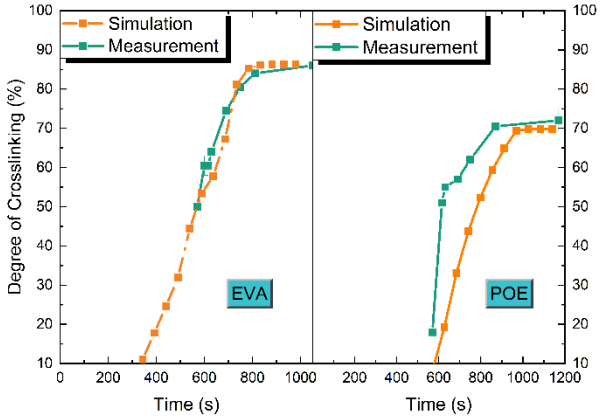

Fig. 10. Simulated and measured degree of crosslinking over time for EVA1 and POE1, glass-backsheet module lay-up

the temperature on both sides approaches the same temperature. When comparing the simulation and measurement, the difference in the temperature profile in the first 300 seconds is noteworthy. In the lamination process shown in Fig. 9 (b), the pins go down and shortly afterwards go up again, causing a direct contact with the heating plate for fast heat transfer. However, after the pins go up, the temperature curve becomes flatter. The short contact of the laminate within the first few seconds and the influence on the temperature was not considered in the simulation. This explains the temperature difference between the measurements and the simulation in the first 300 seconds. The peak temperatures measured on the front and rear side are 154.4 °C and 154.1 °C, while the simulation values are 154.4 °C and 154.5 °C, respectively.

Another point of interest is the measured decrease in temperature between 350 and 400 seconds as in the study of Rahmoun et al. when the module is transferred from HP1 to HP2 [46]. The contact with ambient temperature during this transfer stage caused the small drop in temperature profile. In this study, this transfer stage is simulated to better match simulation results and thermocouple measurements, an improvement over a previous study [47].

E. Degree of Crosslinking Curve

The results of the simulations for EVA and POE are compared with the measurements conducted in our previous study, where we analyzed the degree of crosslinking over time for different curing durations at 150° C (Fig. 10) [2]. For the simulation some parameters were adjusted, such as to fit the used glass thickness and the lamination temperature in this experiment.

When comparing the simulation results with the measurements from our previous study (Fig. 10), we observed a good agreement for both encapsulants, EVA and POE. However, there is a discrepancy in trend over time in the range from 600th second to 850th second, between the simulation and measurements conducted on POE. Despite this discrepancy, it is worth noting that towards the end of the time period analyzed, the simulation and measurement results come closer together, with a difference of approximately 2%, which falls within the range of the error bar. It is also observed that at the end of the lamination process the degree of crosslinking reaches a certain plateau for both, the simulation and measurement, which leads

to the conclusion that the process is long enough to ensure complete curing.

IV. CONCLUSION

In conclusion, this study provides valuable insights into the lamination process for photovoltaic modules and its impact on the crosslinking behavior of different encapsulants. By systematically analyzing module lay-ups, encapsulant materials, and process parameters, several significant findings have emerged.

First, we introduced a method to measure the crosslinking of POE encapsulants. Our investigation into the comparison of the encapsulant crosslinking on the front and rear sides of the module revealed that the degree of crosslinking was 6.5-14.0% lower on the rear side of glass-glass (GG) modules compared to the front side. This indicates a temperature difference between the sides within the plate-membrane lamination process. The difference is attributed to the lower heat transfer at the plate-membrane chamber or the insufficient process time. To address this, we propose active heating on both sides during lamination or extending the process duration. Our conclusion is that it is not recommended to manufacture glass-glass modules in the same chamber and with the same process as glass-backsheet modules. The encapsulant type also plays a significant role, with one EVA consistently exhibiting lower degrees of crosslinking compared to another EVA, whereas a similar trend was observed for POE encapsulant. Therefore, adapting the process to each individual material is crucial to achieve the desired degree of crosslinking.

Moreover, incorporating cells into the laminate led to the observation that the degree of crosslinking decreased by 3.5% to 12.75% based on module lay-up and encapsulant. This shows the influence of cells on the degree of crosslinking and that this factor should not be neglected. Therefore, it is important to include cells in encapsulant tests and in simulations for future studies.

The temperature profile during lamination, analyzed through thermocouple measurements and simulation, exhibited a high degree of conformity between them. Notably, the simulated temperature peaks closely matched the measured values with less than 2 °C difference between simulation and measurement. Additionally, the degree of crosslinking curve, exhibited a commendable alignment with measurements. Although a slight discrepancy for the POE encapsulant, the simulation maintained a satisfactory correspondence, underscoring its practical value.

Overall, these findings shed light on key factors affecting the lamination process and crosslinking behavior in PV modules. They not only enhance our understanding of module manufacturing but also provide a validated simulation tool for predicting crosslinking behavior of various encapsulants. With implications for module quality, reliability, and operational stability, this study provides valuable insights that could help to improve manufacturing processes.

REFERENCES

[1] G. Cattaneo, A. Faes, H. Y. Li, F. Galliano, M. Gragert, Y. Yao, R. Grischke, T. Söderström, M. Despeisse, C, Ballif, A. Perret, E. Laure, "Lamination process and encapsulation materials for glass–glass PV module design," *Photovoltaics International*,

[2] A. K. Schnatmann, F. Schoden, and E. Schwenzfeier-Hellkamp, "Sustainable PV Module Design—Review of State-of-the-Art Encapsulation Methods," Sustainability, vol. 14, no. 16, p. 9971, 2022, doi: 10.3390/su14169971.

[3] A. K. Öz, C. Wellens, M. Mittag, M. Wiese, S. Sraisth, D. Klaus, D. H. Neuhaus, and M. Heinrich, "2.5 Minutes Lamination Process and the Influences of the Degree of Cross-Linking and the Moisture Ingress on the Degradation of PV Modules," 7 pages / 8th World Conference on Photovoltaic Energy Conversion; 816-822: WIP, 2022, doi: 10.4229/WCPEC-82022-3DV.1.12.

[4] C. Barretta, G. Oreski, S. Feldbacher, K. Resch-Fauster, and R. Pantani, "Comparison of Degradation Behavior of Newly Developed Encapsulation Materials for Photovoltaic Applications under Different Artificial Ageing Tests," (eng), Polymers, vol. 13, no. 2, 2021, doi: 10.3390/polym13020271.

[5] G. Oreski, A. Omazic, G. C. Eder, Y. Voronko, L. Neumaier, W. Mühleisen, C. Hirschl, G. Ujvari, R. Ebner, and M. Edler, "Properties and degradation behaviour of polyolefin encapsulants for photovoltaic modules," Progress in Photovoltaics, vol. 28, no. 12, pp. 1277–1288, 2020, doi: 10.1016/j.solmat.2021.110976.

[6] M. Fischer, M. Woodhouse, P. Baliozian, and J. Trube, "International Technology Roadmap for Photovoltaic (ITRPV)," vol. 14, 2023, doi: 10.4229/EUPVSEC20202020-2CV.1.59.

[7] B. Adothu, P. Bhatt, S. Zele, J. Oderkerk, F. R. Costa, and S. Mallick, "Investigation of newly developed thermoplastic polyolefin encapsulant principle properties for the c-Si PV module application," *Materials Chemistry and Physics*, vol. 243, p. 122660, 2020, doi: 10.1016/j.matchemphys.2020.122660.

[8] C. Sen, H. Wang, X. Wu, M. U. Khan, C. Chan, M. Abbott, and B. Hoex, "Four failure modes in silicon heterojunction glass-backsheet modules," *Solar Energy Materials and Solar Cells*, vol. 257, p. 112358, 2023, doi: 10.1016/j.solmat.2023.112358.

[9] P. M. Sommeling, J. Liu, and J. M. Kroon, "Corrosion effects in bifacial crystalline silicon PV modules; interactions between metallization and encapsulation," *Solar Energy Materials and Solar Cells*, vol. 256, p. 112321, 2023, doi:10.1016/j.solmat.2023.112321.

[10] N. T. Dintcheva, E. Morici, and C. Colletti, "Encapsulant Materials and Their Adoption in Photovoltaic Modules: A Brief Review," *Su*stainability, vol. 15, no. 12, p. 9453, 2023, doi:10.3390/su15129453.

[11] R. F. M. Lange, Y. Luo, R. Polo, and J. Zahnd, "The lamination of (multi)crystalline and thin film based photovoltaic modules," Progress in Photovoltaics, vol. 19, no. 2, pp. 127–133, 2011, doi:10.1002/pip.993.

[12] K. Aitola, G. Gava Sonai, M. Markkanen, J. Jaqueline Kaschuk, X. Hou, K. Miettunen, and P. D. Lund, "Encapsulation of commercial and emerging solar cells with focus on perovskite solar cells," Solar Energy, vol. 237, pp. 264–283, 2022, doi: 10.1016/j.solener.2022.03.060.

[13] J. Zhu, G. Surier, D. Wu, D. Montiel-Chicharro, T. R. Betts, and R. Gottschalg, "Adhesion requirements for photovoltaic modules of polymeric encapsulation," in 2016 IEEE International Reliability Physics Symposium (IRPS), Pasadena, CA, USA, 2016, PV-4-1-PV-4-5, doi: 10.1109/IRPS.2016.7574636.

[14] A. K. Öz, C. Herzog, C. Wellens, D. E. Mansour, M. Heinrich, and A. Kraft, "The Impact of the Lamination Process on the Adhesion Properties at the Glass-Encapsulant Interface and Damp Heat Stability of PV Modules. 7 pages / 38th European Photovoltaic Solar Energy Conference and Exhibition; 708-714: WIP, 2021, doi:10.4229/EUPVSEC20212021-4AV.1.5.

[15] S. Sraisth, A. K. Öz, D. Klaus, C. Wellens, and M. Heinrich, Eds., *Influence of the Lamination Pressure on the Adhesion, Degree of Cross-Linking, and Bubble Formation of PV Modules*. 7 pages / 8th World Conference on Photovoltaic Energy Conversion; 823-829: WIP, 2022, doi: 10.4229/WCPEC-82022-3DV.1.17.

[16] G. M. Wallner, B. Adothu, R. Pugstaller, F. R. Costa, and S. Mallick, "Comparison of Crosslinking Kinetics of UV-Transparent Ethylene-Vinyl Acetate Copolymer and Polyolefin Elastomer Encapsulants," (eng), Polymers, vol. 14, no. 7, 2022, doi:10.3390/polym14071441.

[17] M. L. Pliquet, T. Béjat, M. Sérasset, A. Descormes, E. Mofakhami, and E. Voroshazi, "Standardized cross-linking determination methods applied to POE encapsulants in lamination recipe development," 2023, doi: 10.22541/au.169175703.36995479/v1.

[18] C. Hirschl, L. Neumaier, S. Puchberger, W. Mühleisen, G. Oreski, G. C. Eder, R. Frank, M. Tranitz, M. Schoppa, M. Wendt, N. Bogdanski, A. Plösch, and M. Kraft, "Determination of the degree of ethylene vinyl acetate crosslinking via Soxhlet extraction: Gold standard or pitfall?," *Solar Energy Materials and Solar Cells*, vol. 143, pp. 494–502, 2015, doi: 10.1016/j.solmat.2015.07.043.

[19] C. Lux, U. Blieske, E. Malguth, and N. Bogdanski, *Variations in Cross-Link Properties of EVA of Un-Aged and Aged PV-Modules*. 5 pages / 29th European Photovoltaic Solar Energy Conference and Exhibition; 2462-2466 / 29th European Photovoltaic Solar Energy Conference and Exhibition; 2462-2466: WIP, 2014.

[20] International Electrotechnical Commission, *Measurement procedures for materials used in photovoltaic modules*, 1st ed. Geneva, Switzerland: International Electrotechnical Commission, 2017.

[21] C. Hirschl, M. Biebl–Rydlo, M. DeBiasio, W. Mühleisen, L. Neumaier, W. Scherf, G. Oreski, G. Eder, B. Chernev, W. Schwab, and M. Kraft, "Determining the degree of crosslinking of ethylene vinyl acetate photovoltaic module encapsulants—A comparative study," *Solar Energy Materials and Solar Cells*, vol. 116, pp. 203–218, 2013, doi: 10.1016/j.solmat.2013.04.022.

[22] M. Mittag, L. Vogt, C. Herzog, A. Pfreundt, J. Shahid, D. H. Neuhaus, and H. Wirth, "Thermal Modelling of Photovoltaic Modules in Operation and Production," in 3*6th European Photovoltaic Solar Energy Conference and Exhibition; 892-900: WIP, 2019*, doi: 10.4229/EUPVSEC20192019-4CO.2.4.

[23] T. Geipel and U. Eitner, "Cure Kinetics of Electrically Conductive Adhesives," *Energy Procedia*, vol. 38, pp. 340–347, 2013, doi: 10.1016/j.egypro.2013.07.287.

[24] T. Geipel and U. Eitner, "Cure Kinetics of Electrically Conductive Adhesives for Solar Cell Interconnection," *IEEE J. Photovoltaics*, vol. 3, no. 4, pp. 1208–1214, 2013, doi: 10.1016/j.egypro.2013.07.287.

[25] *S-2 Glass Fiber.* [Online] Available: URL: https://www.matweb.com/search/datasheet.aspx?MatGUID=881df8cd9bde4344820202eb6d1e7a39. Accessed on: Dec. 17 2022.

[26] Fibrolux GmbH mposite Thermal Ceramic, *Characteristic values - Fibrolux GmbH.* [Online] Available: URL: https://fibrolux.com/en/characteristic-values/. Accessed on: Mar. 03 2023.

[27] *Air - Thermophysical Properties.* [Online] Available: URL: https://www.engineeringtoolbox.com/air-properties-d_156.html. Accessed on: May 21 2022.

[28] *Silicone Rubber.* [Online] Available: URL: https://www.azom.com/properties.aspx?ArticleID=920. Accessed on: May 21 2022.

[29] *Overview of materials for Polytetrafluoroethylene (PTFE), Extruded.* [Online] Available: URL: https://www.matweb.com/search/datasheet_print. Accessed on: Dec. 18 2022.

[30] *DEC_Tedlar_GeneralProperties.* [Online] Available: URL: https://www.rowlam.com/documents/DEC_Tedlar_GeneralProperties.pdf. Accessed on: May 21 2022.

[31] Torsten Kruse, *"List-Of-Materials-Specific-Heat-Capacity-Ranges.* [Online] Available: URL: https://krusetraining.com/wp-content/uploads/2017/12 / List - Of - Materials - Specific - Heat - Capacity - Ranges . pdf. Accessed on: May 21 2022.

[32] *Ethylene Vinyl Acetate (EVA).*" [Online] Available: URL: https://www.makeitfrom.com/material- properties/Ethylene-VinylAcetate-EVA. Accessed on: May 21 2022.

[33] A. Chamkha and F. Selimefendigil, "Numerical Analysis for Thermal Performance of a Photovoltaic Thermal Solar Collector with SiO2-Water Nanofluid," *Applied Sciences*, vol. 8, no. 11, p. 2223, 2018, doi:10.3390/app8112223.

[34] A. Riverola, A. Mellor, D. Alonso Alvarez, L. Ferre Llin, I. Guarracino, C. N. Markides, D. J. Paul, D. Chemisana, and N. Ekins-Daukes, "Mid-infrared emissivity of crystalline silicon solar cells," *Solar Energy Materials and Solar Cells*, vol. 174, pp. 607–615, 2018, doi: 10.1016/j.solmat.2017.10.002.

[35] *Toughened (Tempered) Soda-Lime Glass.* [Online] Available: URL: https://www.makeitfrom.com/material-properties/Toughened-Tempered-Soda-Lime-Glass. Accessed on: May 21 2022.

[36] I. Subedi, T. J. Silverman, M. G. Deceglie, and N. J. Podraza, "Emissivity of solar cell cover glass calculated from infrared reflectance measurements," *Solar Energy Materials and Solar Cells*, vol. 190, pp. 98–102, 2019, doi: 10.1016/j.solmat.2018.09.027.

[37] EndMemo, *Felt Wool Specific Heat.* [Online] Available: URL: https://endmemo.com/chem/specificheatsearch.php?q=Felt\%20Wool. Accessed on: Dec. 18 2022.

[38] *Woolen Felt Density: 0.35 -1.0 Gram Per Cubic Meter (G/M3) at Best Price in Mumbai.* Honest Enterprise. [Online]. Available: URL: https://www. tradeindia.com/products/woolen-felt-c3451922.html. Accessed on Dec. 18 2022)

[39] *Morgan Advanced Ceramics Min-K K-Shield™ Felt AG Composite Thermal Ceramic.* [Online] Available: URL: https://www.matweb.com/search/DataSheet . aspx ? MatGUID = 611cffd85f5045faa115124f0e4a812f. Accessed on: Dec. 17 2022.

[40] H. L. Friedman, "Kinetics of thermal degradation of char-forming plastics from thermogravimetry. Application to a phenolic plastic," *J. polym. sci., C Polym. symp.*, vol. 6, no. 1, pp. 183–195, 1964, doi: 10.1002/polc.5070060121.

[41] *Activation Energy.* [Online] Available: URL: https://www.chem.fsu.edu/chemlab/chm1046course/activation.html. Accessed on: May 22 2022.

[42] Libretexts, *6.2.3.3: The Arrhenius Law - Activation Energies.* [Online] Available: URL: https://chem.libretexts.org/Bookshelves/Physical_and_Theoretical_Chemistry_Textbook_Maps/Supplemental_Modules_(Physical_and_Theoretical_Chemistry)/Kinetics/06%3A_Modeling_Reaction_Kinetics/6.02%3A_Temperature_Dependence_of_Reaction_Rates/6.2.03%3A_The_Arrhenius_Law/6.2.3.03%3A_The_Arrhenius_Law-_Activation_Energies. Accessed on: May 22 2022.

[43] S. Habibu, N. M. Sarih, N. A. Sairi, and M. Zulkifli, "Rheological and thermal degradation properties of hyperbranched polyisoprene prepared by anionic polymerization," (eng), *Royal Society open science*, vol. 6, no. 11, p. 190869, 2019, doi: 10.1098/rsos.190869

[44] S. Lust, N. Schnitzler, A. Brendler, and S. Wendlandt, "Challenges for Quality Control Posed by New PV Encapsulation Materials," in *WIP-Munich, 2023*.

[45] G. Oreski, C. Barretta, P. Gebhardt, K. A. Weiß, D. C. Miller, S. Uličná, M. Kempe, L. S. Bruckman, L. Gnocchi, H. Li, B. Habersberger, K. Proost, and M. Kühne, "Polyethlylene copolymers as solar cell encapsulants: A critical overview: [To be published]," 2023.

[46] I. Rahmoun, T. Le Carre, B. Chambion, E. Mofakhami, A. Derrier, J.-L. Bouvard, and P.-O. Bouchard, "3-D Modeling of Thermal Exchange in the PV Module During Lamination: Impact of Architecture, Laminator Configuration, and Lamination Recipe," *IEEE J. Photovoltaics*, vol. 12, no. 1, pp. 107–113, 2022, doi: 10.1109/jphotov.2021.3111510.

[47] A. K. Öz, J. Vasani, C. Reichel, C. Wellens, and D. H. Neuhaus, "Temperature Distribution during the Lamination Process of PV Modules and its Influence on the Degree of Crosslinking for EVA-Simulation vs Test Results," (en), *40th European Photovoltaic Solar Energy Conference and Exhibition*, 2023, doi:10.4229/EUPVSEC2023/3AV.1.5.